PROCEEDINGS OF THE ROYAL SOCIETY A

Proc. R. Soc. A (2012) **468**, 1304–1324
doi:10.1098/rspa.2011.0589
Published online 16 January 2012

Instabilities in a drop-strip system: a simplified model

By Marco Rivetti[1,2,*] and Sébastien Neukirch[1,2]

[1]*UPMC Univ Paris 06, and* [2]*CNRS, UMR 7190, Institut Jean Le Rond d'Alembert, 75005 Paris, France*

We study the deformation of an elastic strip by a liquid drop. At small enough scales, capillarity is the dominant fluid effect and surface tension forces may be sufficient to fold the beam, resulting in the wrapping of the drop by the beam. However, wrapping of the drop can be inhibited by the weight of the beam, which creates an energy barrier. The barrier can be overcome by input of kinetic energy in the form of impact of the drop. We introduce a semi-analytical model to study equilibria and their stability in three drop-beam systems: evaporation of a drop wetting and bending an elastic beam; impact of a drop on an elastic beam; lifting of a heavy elastic beam by a drop and we show the model reproduces experimental data. In relevant cases, we use the concept of suddenly applied load to discuss dynamic instabilities.

Keywords: capillarity; one-dimensional elasticity; bifurcation; variational approach

1. Introduction

Classical fluid–structure interactions take place in set-ups where fluid flows apply stress on elastic structures, thereby inducing vibrations of these structures. At small scales and in quasi-static set-ups, surface tension is the source of another type of fluid–structure interaction as an elastic structure may be soft enough to experience strong deformations due to capillary forces (Roman & Bico 2010). Recent examples involve wet filaments forming bundles (Bico *et al.* 2004), liquid–air interfaces buckling an elastic strut (Cohen & Mahadevan 2003; Neukirch *et al.* 2007), liquids rising inside elastic walls and deforming the walls (Kim & Mahadevan 2006; Aristoff *et al.* 2011; Duprat *et al.* 2011), liquid drops deposited on floating thin films and inducing the wrinkling of the film (Huang *et al.* 2007; Vella *et al.* 2010). These *elasto–capillary* interactions appear in a wide range of problems and have been studied intensively over the past few years.

The evaporation of a drop lying on a thin elastic sheet may result in the folding of the sheet around the drop (Py *et al.* 2007). Use of this 'capillary origami' phenomenon has been proposed for the fabrication of three-dimensional photovoltaic cells (Guo *et al.* 2009) or even smaller objects. As a matter of fact, capillary driven self-folding mechanisms have been shown to be useful in the fabrication of microelectromechanical systems (MEMSs) to achieve three-dimensional structures that are otherwise complicated to realize (Gracias

*Author for correspondence (rivetti@ida.upmc.fr).

Received 29 September 2011
Accepted 15 December 2011

et al. 2002; Syms *et al.* 2003; Leong *et al.* 2007; Mastrangeli *et al.* 2009). Recent experiments have shown that elasto-capillary wrapping can be achieved using drop impact on millimetric and centimetric scales (Antkowiak *et al.* 2011). The success of the wrapping has been shown to depend on several parameters, as elasticity, capillarity and gravity all come into play.

In this paper, we develop a model to understand the interactions between these three effects and show that a simple theory can reproduce experimental data and shed light on the wrapping instability. Our goal is to understand the mechanisms underlying the behaviour of the system, predict equilibrium shapes and their stability. We also discuss the differences between static and dynamic instability, the latter involving dynamics of the system and basin of attraction of equilibrium points.

The paper is organized as follows. We first introduce some general hypotheses of our framework in §2, and we then validate our model in §3 with a problem involving only elasticity and capillarity. In §4, we use the concept of suddenly applied load and dynamic stability to show our model can reproduce experimental data, and we give a detailed study on static and dynamic stability of an heavy elastic strip lifted by the capillary action of a drop in §5.

2. Main hypotheses

In this section, we introduce some typical length scales of the problem, explain the simplifications we perform and describe how we compute equilibrium points and their stability.

(*a*) *Different length scales*

Elasticity of structures involves no typical length scale, but once coupled with capillarity or gravity length scales arise. An elastic beam loaded axially will buckle once the force exceeds a threshold. If L is the length of the beam and EI its bending stiffness, the buckling threshold scales like EI/L^2. We note E the Young's modulus and I the second moment of area of the cross section. In the present case of a beam of thickness h and width w, with $h \ll w$, we have $I = h^3 w/12$, and the beam preferentially bends in the plane orthogonal to w. If the extremity of such a beam is brought to contact with a liquid–air interface, then capillary forces scaling like $2(h + w)\gamma \simeq 2\gamma w$ are exerted, where γ is the surface energy of the interface. Such forces are sufficient to induce buckling if $L \gtrsim L_{\mathrm{ec}}$, with

$$L_{\mathrm{ec}} = \sqrt{\frac{EI}{\gamma w}}, \tag{2.1}$$

where L_{ec} is referred to as the elasto-capillary length (Cohen & Mahadevan 2003; Bico *et al.* 2004).

In the same manner, equating buckling forces with the total weight of the beam, we introduce the gravito-elastic length, L_{eg}

$$L_{\mathrm{eg}} = \left(\frac{EI}{\rho g h w}\right)^{1/3}, \tag{2.2}$$

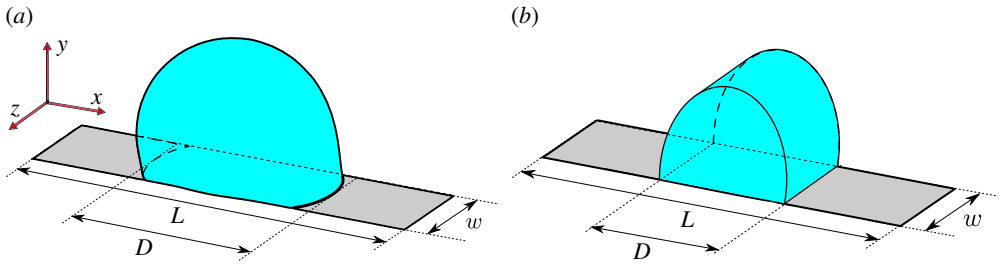

Figure 1. A liquid drop lies on a rigid rectangular surface. (*a*) Solution of the surface evolver (Brakke 1992) problem and (*b*) the approximation used here, where the liquid–air interface is cylindrical. (Online version in colour.)

where ρ is the density of the beam and g is the acceleration of gravity. Beams that are longer than L_{eg} are significantly deformed by gravity.

In this paper, we concentrate our attention on the problem of a drop lying on a slender beam. On the one hand, the radius R of the drop has to be larger than L_{ec} to observe significant bending. On the other hand, drop radius is limited by gravity and one has to keep $R < L_{\mathrm{gc}}$ for the drop to remain spherical, $L_{\mathrm{gc}} = (\gamma/\rho_{\mathrm{L}} g)^{1/2}$ being the gravito-capillary length (here ρ_{L} denotes the liquid density). Therefore, we work with drops of radii $L_{\mathrm{ec}} < R < L_{\mathrm{gc}}$, neglecting the weight of the drop, and also its inertia and viscosity.

(*b*) *Two-dimensional model of a three-dimensional problem*

In the physical problem we consider, the drop profile is roughly a spherical cap and the strip behaves as an elastic plate because its thickness h is very small when compared with its other two dimensions (w, L). Therefore, we face a native three-dimensional problem and a complete resolution would necessitate complex numerics solving both liquid and solid phases. The goal of this study being to find a simple model predicting the general behaviour of the system, we introduce several simplifications of the problem.

First of all as $h \ll w \ll L$ (figure 1), one expects bending in the x–y plane to be dominant with respect to other planes. Invariance in the z-direction leads to consider the strip as a (one-dimensional) beam. Even if the strip is invariant in the z-direction, the drop still has a three-dimensional shape. However, as we will introduce an energy-based model, only the area of the liquid–air interface will matter. As the width w of the strip is chosen to be somewhat smaller than the drop size, the drop will primarily extend in the x–y plane, leaving the z-direction approximatively invariant. We therefore approximate the shape of the drop with a cylindrical surface, invariant in the z-direction and bounded by two planar caps (figure 1). In order to asses the approximation involved in this simplification, we numerically solve, using *surface evolver* (Brakke 1992), for the shape and area of a drop of volume V constrained to lie on a rigid flat strip of length D and width w. For several combinations of V, w and D, we compare the extent of the liquid–air interface given by the simulation with that of a cylindrical drop and we find that, even if the cylindrical drop always has a larger area, then the ratio between the area of the three-dimensional shape and the cylindrical surface

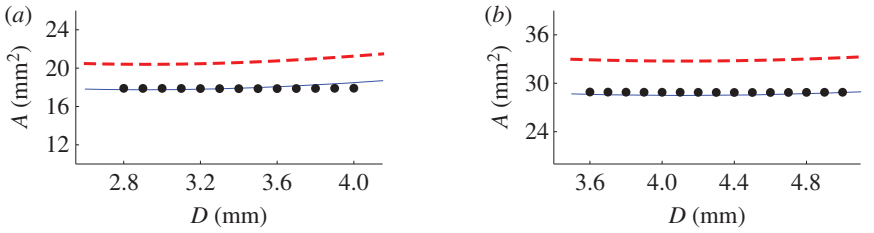

Figure 2. Area of the liquid–air interface for a three-dimensional drop calculated with *surface evolver* (discs) and with the cylindrical interface approximation (dashed line), as function of the drop base extent D. Parameters are: width $w = 3\,\mathrm{mm}$ and liquid volumes (*a*) $V = 10\,\mathrm{mm}^3$ and (*b*) $V = 20\,\mathrm{mm}^3$. Solid line is obtained by scaling the dashed line by a corrective factor 0.87. (Online version in colour.)

(plus caps) does not vary much with parameters. In the parameter range we are interested in, a good approximation is $A_{\text{three-dimensional}}/A_{\text{cyl}} \simeq 0.87$ (figure 2). In §4, where we compare our model results with experimental data, we use this correction coefficient, making the further hypothesis that it does not change as the strip bends.

(*c*) *Discrete energy approach*

We use an energy approach to find equilibrium shapes and their stability. Total potential energy $\mathcal{E}$ of the system is given by the sum of elastic ($\mathcal{E}_{\text{el}}$), capillary ($\mathcal{E}_\gamma$) and gravitational ($\mathcal{E}_{\text{g}}$) energies. In the case of a one-dimensional beam problem, this could be formally written as

$$\mathcal{E} = \mathcal{E}_{\text{el}} + \mathcal{E}_\gamma + \mathcal{E}_{\text{g}} = \int_{\text{beam}} \mathcal{F}(x(s), y(s), \varphi(s))\,\mathrm{d}s, \tag{2.3}$$

where $(x(s), y(s))$ is the deformed position of the beam in the plane, $\varphi(s)$ is the angle between the horizontal axis and the tangent of the beam, and $\varphi'(s) = \kappa(s)$ is the curvature of the beam. The variable s is the arc-length along the beam. Looking for stationary points of this functional leads to classical Euler–Lagrange equations. This exact resolution requires to solve a system of differential equations with boundary conditions. In order to simplify the problem, we strongly restrict the functional space in which the unknown functions $(x(s), y(s), \varphi(s))$ live, that is we choose the shape of the deformations, leaving amplitudes unknown. This Galerkin-type reduction is performed in such a way that the kinematics and physical constraints are satisfied. The unknown function $\kappa(s)$ is, for example, approximated as

$$\kappa(s) = \sum_{i=1}^{n} c_i \psi_i(s), \quad i = 1, 2, \ldots, n, \tag{2.4}$$

where the basis functions $\psi_i(s)$ are given. This introduces unknown variable coefficients c_i and changes the total energy (2.3) from being a functional to being a mere function of the c_i: $\mathcal{E} = \mathcal{E}(\mathbf{c})$, with $\mathbf{c} = (c_1, c_2, \ldots, c_n)$. Looking for

extremums of the energy (i.e. equilibrium points) now requires to solve only a (possibly nonlinear) system of equations

$$\frac{\partial \mathcal{E}}{\partial \mathbf{c}} = \mathbf{0}. \tag{2.5}$$

In the problems considered in the following sections, we minimize $\mathcal{E}(\mathbf{c})$ in the presence of m constraints $\phi_\alpha(\mathbf{c}) = 0$, $\alpha = 1, 2, \ldots, m$. We therefore introduce Lagrange multiplier(s) λ_α and the Lagrangian function $\mathcal{L} = \mathcal{E} - \sum_\alpha \lambda_\alpha \phi_\alpha$. Lagrangian multipliers add new equilibrium equations to the system

$$\frac{\partial \mathcal{L}}{\partial \mathbf{c}} = \mathbf{0} \quad \text{and} \quad \frac{\partial \mathcal{L}}{\partial \lambda_\alpha} = 0 \quad \forall \alpha. \tag{2.6}$$

Once an equilibrium point $\mathbf{c}^0$ satisfying the constraints $\phi_\alpha(\mathbf{c}^0) = 0$ $\forall \alpha$ is found, we test its stability. The equilibrium solution $\mathbf{c}^0$ is said to be stable, if it locally minimizes $\mathcal{E}$ among all admissible variations $\mathbf{c} = \mathbf{c}^0 + \epsilon \delta \mathbf{c}$:

$$\mathcal{E}(\mathbf{c}^0) < \mathcal{E}(\mathbf{c}^0 + \epsilon \delta \mathbf{c}) \quad \forall \delta \mathbf{c} \quad \text{such that} \quad \phi_\alpha(\mathbf{c}^0 + \epsilon \delta \mathbf{c}) = 0 \quad \forall \alpha, \tag{2.7}$$

where $\epsilon \ll 1$. A variation $\delta \mathbf{c}$ is said admissible if $\phi_\alpha(\mathbf{c}^0 + \epsilon \delta \mathbf{c}) = 0$. Because we already have $\phi_\alpha(\mathbf{c}^0) = 0$, this requires $\delta \mathbf{c} \cdot \partial \phi_\alpha / \partial \mathbf{c} = 0$, $\forall \alpha$. Consequently, we compute the Hessian matrix

$$H = \frac{\partial^2 \mathcal{L}}{\partial \mathbf{c}\, \partial \mathbf{c}} \tag{2.8}$$

and evaluate $H^0 = H(\mathbf{c}^0)$. Stable solutions are such that $\delta \mathbf{c} \cdot H^0 \cdot \delta \mathbf{c} > 0$ for all admissible variations $\delta \mathbf{c}$. It can be shown that this is equivalent to having only positive eigenvalues for the 'projected' Hessian (Luenberger 1973)

$$H' = K^T \cdot H^0 \cdot K, \tag{2.9}$$

where the columns of the matrix K are the vectors of the basis of the kernel of the matrix whose lines are $\partial \phi_\alpha / \partial \mathbf{c}$. The 'projected' Hessian H' is a square matrix of dimension $(n - m) \times (n - m)$.

3. Evaporation of a drop bound to an elastic strip

In figure 3, a liquid drop is brought into contact with an elastic strip of length L. Surface tension tends to make the drop circular, thereby bending the strip and resulting in a trade-off between elastic and capillary energies. As the drop evaporates, the quasi-static evolution of the system is monitored and the final configuration of the system depends on the ratio L/L_{ec} (Py *et al.* 2007). We show that our simplified discrete model can capture the different responses of the system, allowing us to draw bifurcation diagrams and give an approximation value for the threshold ratio L/L_{ec} computed by Py *et al.* (2007) with the continuous model. As in Py *et al.* (2007), the gravitational energy is not considered here.

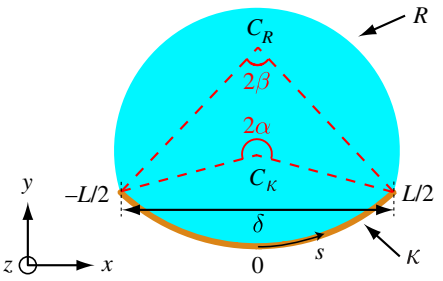

Figure 3. Model for the capillary adhesion of a drop and an elastic strip. The strip has length L and constant curvature κ. The interface between the drop and the air has curvature $1/R$. The system is invariant along the direction z and has depth w. The shaded (blue) region has area A_c, see equation (3.3). (Online version in colour.)

(*a*) *Model*

As shown in figure 3, in the present model, the strip centre line is a circular arc of radius $1/\kappa$, centre C_κ and central angle 2β; the liquid–air interface is a circular arc of radius R, centre C_R and central angle 2α. In this approximation of uniform curvature κ, the elastic deformation energy of the elastic strip is then

$$\mathcal{E}_{\mathrm{el}} = \frac{1}{2}\int_{-L/2}^{L/2} EI\kappa^2(s)\,\mathrm{d}s = \frac{1}{2}EI\kappa^2 L. \tag{3.1}$$

During evaporation of the liquid, the drop remains pinned to the extremities of the elastic strip, leaving the area of the liquid–solid interface constant. We then have to consider only the energy of the liquid–air interface. In our cylindrical model approximation (figure 1), this interface consists of three parts: the arc of cylinder (of axis z and radius R) from $s=-L/2$ to $s=+L/2$, and the two planar caps in the x–y plane, bounded by the strip and the circular arc of radius R (figure 3). The interface energy is then

$$\mathcal{E}_\gamma = \iint_{\partial V} \gamma\,\mathrm{d}A = \gamma(2\alpha wR + 2A_c), \tag{3.2}$$

where A_c is the area of a planar cap

$$A_c = \frac{1}{\kappa^2}\left(\beta - \frac{\sin 2\beta}{2}\right) + R^2\left(\alpha - \frac{\sin 2\alpha}{2}\right). \tag{3.3}$$

The total energy of the system is

$$\mathcal{E}(\kappa,\alpha,\beta,R) = \mathcal{E}_{\mathrm{el}} + \mathcal{E}_\gamma. \tag{3.4}$$

We make use of the two geometric constraints $(1/\kappa)\sin\beta = R\sin\alpha$ and $L = 2\beta/\kappa$ (figure 3) to reduce the set of variables to $\{\kappa,\alpha\}$. For each fixed value V_i of the liquid volume $V = wA_c(\kappa,\alpha)$, we look for stable equilibrium solutions

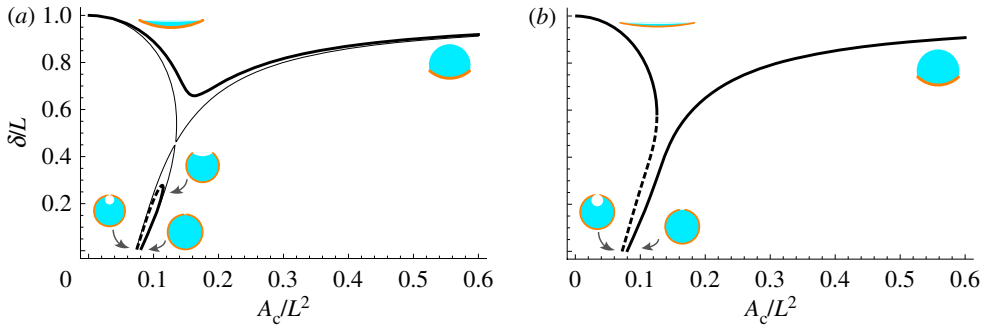

Figure 4. Bifurcation diagram for system in figure 3. The distance δ between the two ends of the strip is plotted as a function of liquid volume $V = A_c w$. Paths of stable (solid curves) and unstable (dashed curves) configurations are shown. (a) Thick curves are for $L = 3.9\, L_{ec}$ for which evaporation ends with an open system. Thin lines are for the limiting case $L = 4.09\, L_{ec}$. (b) Case with $L = 4.2\, L_{ec}$ where evaporation ends with an encapsulated system. (Online version in colour.)

by minimizing the energy $\mathcal{E}$ under the constraint $\phi = V - V_i = 0$, using the Lagrangian $\mathcal{L} = \mathcal{E} - \lambda\phi$

$$\mathcal{L}(\kappa, \alpha) = \frac{1}{2} EI\kappa^2 L + 2\gamma\alpha w \frac{\sin(L\kappa/2)}{\kappa \sin\alpha} - \lambda(wA_c(\kappa, \alpha) - V_i), \tag{3.5}$$

where the constant $2\gamma A_c$ has been removed. Equilibria are found by numerically solving equation (2.6), here $(\partial/\partial\kappa, \partial/\partial\alpha, \partial/\partial\lambda)\mathcal{L} = 0$, and their stability is assessed with the corresponding projected Hessian matrix.

(b) *Results*

Equilibria and stability are shown in figure 4, where the distance δ between the extremities of the strip is plotted as a function of the liquid volume. As already shown in Py *et al.* (2007), depending on the ratio L/L_{ec}, two different behaviours exist during evaporation of the drop. We start with a drop gently bending the strip (large values of $A_c = V/w$) and let evaporation take place (i.e. decreasing A_c). On the one hand, when L/L_{ec} is small, the strip first starts to bend but eventually becomes flat as the volume vanishes (figure 4a). On the other hand, if L/L_{ec} is large enough, the strip progressively bends and the liquid–air interface decreases to finally vanish when the extremities of the strip touch, like the right-most curve of figure 4b. The transition between these two regimes happens at $L = 4.09\, L_{ec}$ (thin line in figure 4a), where a transcritical bifurcation takes place. The present value is an approximation of the value found in the full resolution, $L = 3.54\, L_{ec}$ Py *et al.* (2007). A similar model was introduced by de Langre *et al.* (2010), where a more distant value of the threshold $L = \sqrt{2}\pi L_{ec} \simeq 4.44\, L_{ec}$ was obtained by merely comparing energies of closed and open configurations.

We conclude that our discrete model is precise enough to capture instabilities and bifurcations of drop-strip systems, and we now use it to compute the encapsulation threshold of an impacting drop.

4. Encapsulation of an impacting drop

In Antkowiak *et al.* (2011), a water droplet of volume V_0 falls and impacts a strip lying on a rigid support. The impact point lies at distance L from the right end of the strip, and at distance L' from the left end, with $L' \gg L$. These authors study the influence of the impact velocity U and of the length of the free end L on the final configuration of the system. Two different final states exist: (i) an encapsulated state where the free end of the strip has flipped over and wrapped the drop and (ii) an open state in which the strip is only slightly deformed by the drop.

We use our discrete model to predict the final state of the drop-strip system with an energy criterion. It was shown in Antkowiak *et al.* (2011) that the three-dimensional experiment could be correctly described with two-dimensional calculations. During impact, the drop spreads on the strip until it reaches a maximum extent Δ. At this point, most of the initial kinetic energy has been transformed into surface energy (Clanet *et al.* 2004; Eggers *et al.* 2010), and it is experimentally observed that the contact line will not recede but will remain pinned to the strip (Antkowiak *et al.* 2011). As a consequence, capillary forces, striving for a reduction of the extent of the liquid–air interface, tend to fold the strip, thereby increasing the elastic energy. Moreover, as the strip flips over the drop, gravitational energy of the strip is also increased. This amount of elastic and gravitational energy acts as an energy barrier that has to be compared with the initially available kinetic energy in order to predict the final state of the system.

(*a*) *Model*

In the experimental set-up (Antkowiak *et al.* 2011), the maximal extent of the drop Δ is related to impact velocity U with the empirical law

$$\frac{\Delta - \Delta_0}{2R} = 0.32\, We^{1/2}, \tag{4.1}$$

where $We = \rho R U^2/\gamma$ is the Weber number and Δ_0 is the extent of the wet region when $U = 0$. In subsequent dynamics, the contact line never recedes and may advance only if the dynamic contact angle θ reaches the critical value θ^*. We therefore have $D = \Delta/2$ as long as $\theta < \theta^*$ (see figure 5 for notations). Moreover, as the length $L' - D$ is very large, the left-end tail is considered immobile. Impact of the drop and dynamics of the system take place in milliseconds and, therefore, the volume V of the drop stays constant, $V = V_0$, as no evaporation occurs.

As in §4, the liquid–air interface is a circular arc of radius R, centre C_R and central angle 2α (figure 5).

However, in the present model, the strip has total length $(L + L')$ and is only partly wetted. The left tail $s \in (-L'; -D)$ lies flat on a rigid support, whereas the wetted part $s \in (-D; D)$ and the right tail $s \in (D; L)$ are free to move. In the wetted region, the strip centre line is a circular arc of radius $1/\kappa$, centre C_κ and central angle 2β. The right tail is a straight segment of inclination 2β. As configurations are symmetric with regard to the axis passing through points C_R and C_κ, the wetting angle θ (between the strip and the liquid–air interface) is

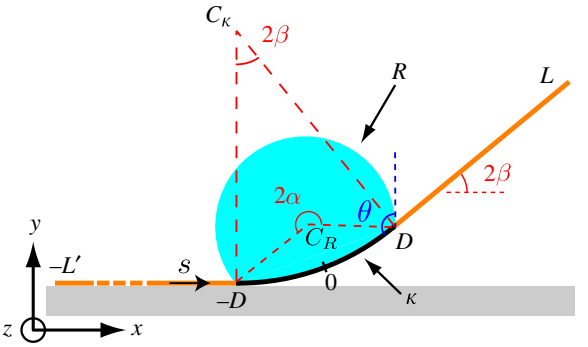

Figure 5. Model of a drop partially wetting an elastic strip. The strip, of length $L + L'$, has uniform curvature κ in the wetted region, and is straight otherwise. The liquid–air interface has uniform curvature $1/R$. The Young contact angle θ is equal to $\alpha + \beta$. The weight of the strip is accounted for and a rigid support prevents the system from globally falling down. The system is invariant along the z direction and has depth w. (Online version in colour.)

the same at $s = D$ and at $s = -D$. The elastic deformation energy of the elastic strip is then

$$\mathcal{E}_{\mathrm{el}} = \frac{1}{2}\int_{-D}^{D} EI\kappa^2(s)\,\mathrm{d}s = EI\kappa^2 D. \tag{4.2}$$

The weight of the strip, responsible for the energy barrier, is now accounted for. The elevation of the strip in the three different regions is

$$y_1(s) = 0 \quad \text{for } s \in (-L'; -D), \tag{4.3}$$

$$y_2(s) = \frac{1 - \cos(\kappa s + \kappa D)}{\kappa} \quad \text{for } s \in (-D; D) \tag{4.4}$$

and

$$y_3(s) = \frac{1 - \cos(2\kappa D)}{\kappa} + (s - D)\sin(2\kappa D) \quad \text{for } s \in (D; L). \tag{4.5}$$

We integrate to obtain the gravitational energy ($\mathcal{E}_{\mathrm{g}}$)

$$\begin{aligned}\frac{\mathcal{E}_{\mathrm{g}}}{\rho g w h} &= \int_{-L'}^{-D} y_1(s)\,\mathrm{d}s + \int_{-D}^{D} y_2(s)\,\mathrm{d}s + \int_{D}^{L} y_3(s)\,\mathrm{d}s \\ &= \frac{1}{\kappa}\left(2D - \frac{\sin(2\kappa D)}{\kappa}\right) + \frac{1 - \cos(2\kappa D)}{\kappa}(L - D) + \frac{1}{2}(L - D)^2\sin(2\kappa D).\end{aligned} \tag{4.6}$$

As in §4, we employ a cylindrical approximation for the drop so that the liquid–air interface comprises three parts: the arc of cylinder (of axis z and radius R) from $s = -D$ to $s = D$, and the two planar caps in the x–y plane, bounded by the strip and the circular arc of radius R (figure 5). As the contact line may move, we also have to consider the surface energy $2\gamma_{\mathrm{sl}} D w$ associated with the solid–liquid interface (spanning from $s = -D$ to $s = +D$) as well as the surface energy $\gamma_{\mathrm{sv}} w(L - D) + \gamma_{\mathrm{sv}} w(L' - D)$ associated with the solid–air interface, for $|s| \geq D$.

Then, the surface energy can be written as

$$\begin{aligned}\mathcal{E}_\gamma &= 0.87 \iint_{\partial V} \gamma \, \mathrm{d}A + 2\gamma_{\mathrm{sl}} D w + \gamma_{\mathrm{sv}}(L + L' - 2D)w \\ &= 0.87\gamma(2\alpha R w + 2A_{\mathrm{c}}) - 2\gamma D w \cos\theta_Y + \gamma_{\mathrm{sv}}(L + L')w, \end{aligned} \tag{4.7}$$

where we make use of the Young construction $\gamma_{\mathrm{sv}} - \gamma_{\mathrm{sl}} = \gamma \cos\theta_Y$, where θ_Y is the static contact angle. Note the presence of the 0.87 correction factor introduced in §2*b*. The two constant terms $\gamma_{\mathrm{sv}} w(L + L')$ and $2 \times 0.87\gamma A_{\mathrm{c}}$ are withdrawn from the energy expression. Adding the energies (4.2), (4.6) and (4.7), we obtain

$$\mathcal{E}(\alpha, \beta, R, \kappa, D) = \mathcal{E}_{\mathrm{el}} + \mathcal{E}_{\mathrm{g}} + \mathcal{E}_\gamma. \tag{4.8}$$

We have to study the energy $\mathcal{E}$ subjected to the following constraints. The first two constraints are geometrical relations linking the variables, namely $(1/\kappa)\sin\beta = R\sin\alpha$, $D = \beta/\kappa$. These two relations are used to eliminate κ and R from the energy (4.8). The constraint of constant liquid volume, $V = A_{\mathrm{c}}$ and $w = V_0$ with A_{c} given by equation (3.3), is used to (numerically) eliminate the variable α from the energy. The energy (4.8) is then a function of the two remaining variables: $\mathcal{E} = \mathcal{E}(\beta, D)$. The last constraint is due to the the pinning of the contact line. Pinning of the contact line happens whenever a drop is deposited of a non-ideal surface where chemical and physical defects are present. In this case, the static contact angle θ is not unique and takes values in an interval around θ_Y, that is, the contact line is immobile as long as θ remains larger than the receding angle and smaller than the advancing angle (de Gennes 1985). In our case, we never observed retraction of the contact line, and will consider only its advancing when θ reaches $\theta^\star$, the advancing contact angle. We introduce the distance D^*, which is the extent of the wet region at the beginning of the dynamics when the strip is flat, computed from equation (4.1) with $D^* = \Delta/2$. The contact angle is $\theta = \alpha + \beta$ and the pinning leads to $D = D^*$ as long as $\theta < \theta^*$. Furthermore, we assume that once the contact line advances, the angle is constant and equal to θ^* (de Gennes 1985). This can be summarized in the form $(D - D^*)(\theta^* - \theta) = 0$, where we have to be careful that both terms must be positive when not zero: the contact angle cannot exceed θ^* and the contact line never retracts. This last constraint makes the energy $\mathcal{E}$ a function of only one variable: $\mathcal{E} = \mathcal{E}(\beta)$ with D either given by $D = D^*$ (during contact line pinning) or solved from $\alpha(\beta, D) + \beta = \theta^*$ (during advancing of the contact line).

(*b*) *Results*

We start our study of the evolution of the system right after the maximal spreading of the impacting drop. There, the kinetic energy is zero, and we compute the potential energy $\mathcal{E}(\beta)$ and use its graph to predict the final state of the system. The impact of the drop is viewed as a suddenly applied load (Simitses & Hodges 2006, ch. 12), and we look for basin of attraction of final states in the presence of dissipation. This dynamical point of view is different from the one seen in §3, where we were looking at a quasi-static succession of equilibrium points, during evaporation. The strip starts its dynamics $\beta = \beta(t)$ (t is physical time) with no speed (i.e. no kinetic energy) at the flat configuration $\beta(0) = 0$, evolves and eventually reaches its final state, either flat $\beta(+\infty) = 0$, folded around

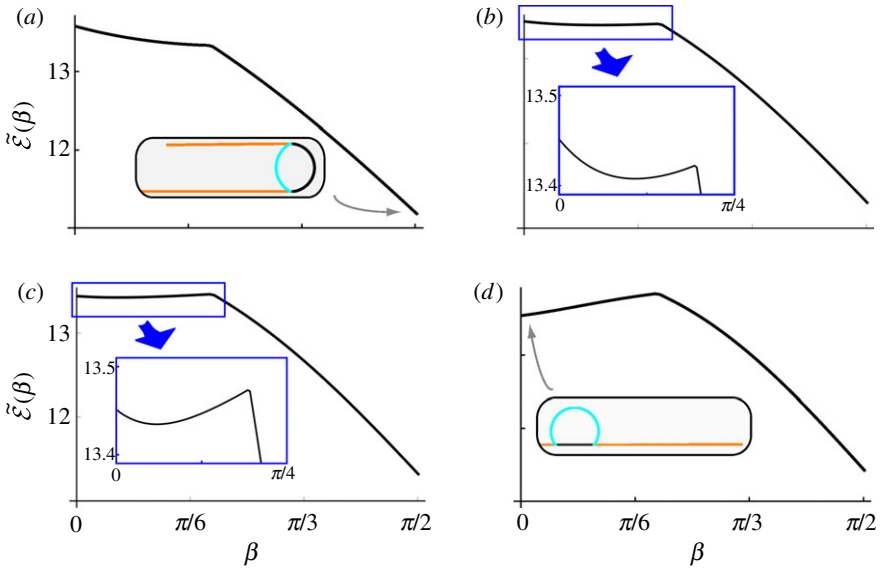

Figure 6. Non-dimensional total energy $\tilde{\mathcal{E}}(\beta) = \mathcal{E} L_{ec}/EI$ for a drop with $V = 92.4\, L_{ec}^3$ and $D^* = 2.93\, L_{ec}$, for different lengths: (*a*) $L = 15.0\, L_{ec}$, (*b*) $L = 18.4\, L_{ec}$, (*c*) $L = 19.2\, L_{ec}$, and (*d*) $L = 22.8\, L_{ec}$. Insets in (*a*) and (*d*) give the shape of the system at the final state, whereas insets in (*b*) and (*c*) show a zoom of the energy curve. (Online version in colour.)

the drop $\beta(+\infty) = \pi/2$ (encapsulated configuration) or in an intermediate state. The level $\mathcal{E}(0)$ represents the initial total mechanical energy of the system and as we here assume the presence of a small amount of dissipation, $\mathcal{E}(t) \leq \mathcal{E}(0)$ for all time t. As we do not compute the time evolution of the system, we do not give any information on the duration of the encapsulation time, but we nevertheless show that we can predict the asymptotic dynamics ($t \to +\infty$) of the system. We use experimentally measured $\theta_Y = 110°$ and $\theta^* = 150°$. We use $L_{ec} = 0.55$ mm and $L_{eg} = 3.6$ mm (Antkowiak *et al.* 2011).

Figure 6 shows the shape of the total potential energy $\mathcal{E}(\beta)$ for given volume $V = 92.4\, L_{ec}^3$ and wetted region extent $D^* = 2.93\, L_{ec}$, and for four different values of the length $L = 15.0$, 18.4, 19.2, and 22.8 L_{ec}. Energy curves all exhibit a tip point at $\beta \simeq 0.6$. Before the tip point, the constraint $D = D^*$ is active and $\theta < \theta^*$; after the tip point, the constraint $\theta = \theta^*$ is active and $D > D^*$. As the volume of the drop has been chosen in such a way that its radius exceeds the elasto-capillary length, all curves have their global energy minimum for the encapsulated state $\beta = \pi/2$. Nevertheless, we see in the following that in some cases there can be alternative stable final state and that an energy barrier can arise. In the first case (figure 6*a*), the global maximum is at $\beta = 0$. The system then starts its dynamics with a flat configuration $\beta = 0$, accelerates and reaches the final state $\beta = \pi/2$ where the strip encapsulate the drop. In the second case (figure 6*b*), an intermediate stable equilibrium state lies at $\beta \simeq 0.35$, corresponding to a open configuration. As the global energy maximum still lies at $\beta = 0$, the system will pass the tip point and evolves towards the state at $\beta = \pi/2$, provided dissipation is not too strong. In the third case (figure 6*c*), there still is an intermediate equilibrium state (at $\beta \simeq 0.2$) and this time the energy level of the tip point is above the energy level

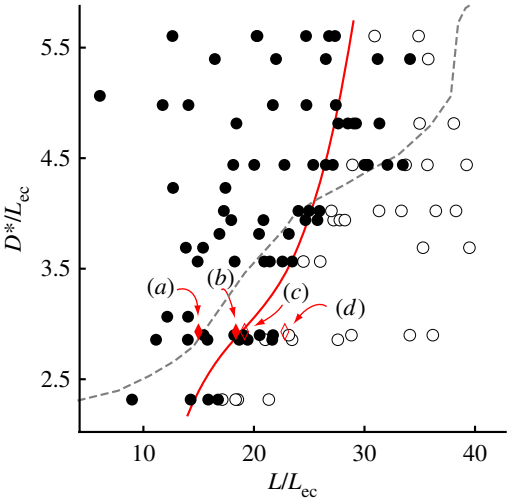

Figure 7. Comparison between theoretical and experimental phases diagram. Experiments: filled circles (respectively, open circles) correspond to encapsulated (respectively, non-encapsulated) final states. Model: solid line is the boundary between the two final states. Rhombs situate the four configurations described in figure 6. The dotted curve corresponds to the boundary found in Antkowiak *et al.* (2011) using numerical simulations. (Online version in colour.)

of the origin. In this case, the initial mechanical energy is not large enough for the system to achieve encapsulation. The final state of the system will be at $\beta \simeq 0.2$, on the intermediate equilibrium state. In the fourth case (figure 6*d*), no intermediate equilibrium exists and as the slope of the energy curve is strictly positive at the origin, the system will not depart from $\beta = 0$.

In conclusion, we use the following criterion: encapsulation occurs if the origin is the global maximum of the energy $\mathcal{E}(\beta)$, and we plot in figure 7 the threshold between encapsulated and open final states as function of the length L and of the initial extent of the wet region D^*. We compare our theoretical curve with the experimental data of Antkowiak *et al.* (2011) and find good agreement. Also shown on the figure are the four cases (a)–(d) of figure 6 with the threshold curve passing between cases (b) and (c). Finally, we note that the agreement between experiment and model is less good when $L/L_{ec} > 25$: for such L, the hypothesis of straight tail is clearly violated as the beam become largely bent in the tail region $s \in (D; L)$, owing to its own weight. Consequently, the gravitational barrier computed with the present model is too large, resulting in a threshold curve being too pessimistic.

5. Drop lifting a heavy elastic strip

In previous sections, we first studied the competition between capillary and elastic energies (§3), and we then introduced the gravitational energy of the strip and used the concept of dynamical instability (§4). We now consider a heavy elastic strip that deforms under capillarity and gravity (figure 8), and we discuss the difference between static and dynamic instabilities.

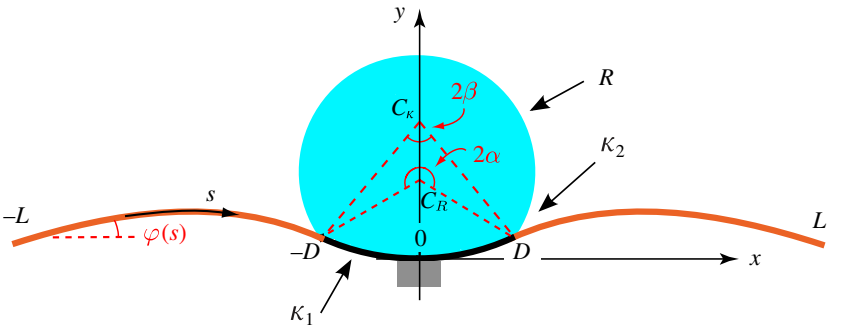

Figure 8. An elastic strip of length $2L$ is bent by capillary forces and self-weight. The drop is wetting the strip along a fixed distance $2D$. The model for the deformation of the elastic strip is such that the curvature is uniform in the wetted region $s \in (-D; D)$ and linearly decreasing in the two dry regions $s \in (D; L)$ and $s \in (-L; -D)$. (Online version in colour.)

(*a*) *Model*

The strip is divided into two regions (i) a wetted region that has uniform curvature and (ii) a dry region with linearly decreasing curvature. Both regions are subjected to gravity. The wet part spans over $s \in (-D; D)$, and for simplicity, we work with strong contact line pinning and keep D fixed, irrespective of the contact angle. Finally, we consider only shapes symmetric on the y-axis, and we fix the point $s = 0$ at the origin, thereby preventing the entire system from falling down during the energy minimization procedure. As in §4, the wetted region, $s \in (-D; D)$, is a circular arc of radius $1/\kappa_1$, centre C_κ and central angle 2β (figure 8). For the first region, the elastic and gravitational energies are as follow

$$\mathcal{E}_{\mathrm{el},1} = 2\int_0^D \frac{1}{2} EI\kappa_1^2 \,\mathrm{d}s = EID\kappa_1^2 \tag{5.1}$$

and

$$\mathcal{E}_{\mathrm{g},1} = 2\int_0^D \rho g S y(s) \,\mathrm{d}s = 2\rho g S \frac{\kappa_1 D - \sin(\kappa_1 D)}{\kappa_1^2}. \tag{5.2}$$

For the second region, the approximation of straight tails was used in §4, valid in the case of short tails $(L - D) \ll L_{\mathrm{eg}}$. We here relax this constraint and for $s \in (D; L)$ (and symmetrically for $s \in (-L; -D)$), we assume a shape where curvature $\kappa(s)$ varies linearly from $\kappa(D) = \kappa_2$ to $\kappa(L) = 0$, zero curvature at $s = \pm L$ being consistent with the absence of external moment at the strip ends. The curvature in this second region then reads

$$\kappa(s) = \frac{\kappa_2(L - s)}{L - D}. \tag{5.3}$$

The deflection angle $\varphi(s)$ and height of the strip $y(s)$ are then found by integrating $\varphi'(s)=\kappa(s)$ and $y'(s)=\sin\varphi(s)$. We obtain

$$\varphi(s)=\frac{\pi}{2}\left(\frac{L-s}{c_1}\right)^2+c_2,\quad \text{with } c_1=\sqrt{\frac{\pi(D-L)}{\kappa_2}}\quad\text{and}\quad c_2=\beta-\frac{1}{2}\kappa_2(D-L) \tag{5.4}$$

and

$$\begin{aligned} y(s)=\frac{1-\cos\beta}{\kappa_1}&-c_1\cos c_2\left[\mathcal{S}\left(\frac{L-s}{c_1}\right)-\mathcal{S}\left(\frac{L-D}{c_1}\right)\right]\\ &-c_1\sin c_2\left[\mathcal{C}\left(\frac{L-s}{c_1}\right)-\mathcal{C}\left(\frac{L-D}{c_1}\right)\right], \end{aligned} \tag{5.5}$$

where these formulas have been written for $\kappa_2<0$ (similar formulas can be written in the case $\kappa_2>0$), and where $\mathcal{S}(x)=\int_0^x\sin(\pi y^2/2)\,\mathrm{d}y$ and $\mathcal{C}(x)=\int_0^x\cos(\pi y^2/2)\,\mathrm{d}y$ are Fresnel integrals. The elastic and gravitational energies for the second region are then

$$\mathcal{E}_{\mathrm{el},2}=2\int_D^L\frac{1}{2}EI\kappa^2(s)\,\mathrm{d}s=\frac{1}{3}EI(L-D)\kappa_2^2 \tag{5.6}$$

and

$$\begin{aligned} \mathcal{E}_{\mathrm{g},2}&=2\int_D^L\rho gSy(s)\,\mathrm{d}s\\ &=2\rho gS(L-D)\left(\frac{1}{\kappa_1}(1-\cos\beta)+\frac{1}{\kappa_2}\left[\cos\beta-\cos\left(\beta+\frac{1}{2}\kappa_2(L-D)\right)\right]\right). \end{aligned} \tag{5.7}$$

As in the previous sections, the liquid–air interface is a circular arc of radius R, centre C_R and central angle 2α (figure 8). In the present case of strong contact line pinning, where the wet region spans from $s=-D$ to $s=+D$ irrespective of the contact angle, the surface energy simplifies to

$$\mathcal{E}_\gamma=2\gamma\alpha Rw, \tag{5.8}$$

adding the energies (5.1), (5.2), (5.6), (5.7), and (5.8), we obtain

$$\mathcal{E}(\alpha,\beta,R,\kappa_1,\kappa_2)=\mathcal{E}_{\mathrm{el},1}+\mathcal{E}_{\mathrm{g},1}+\mathcal{E}_{\mathrm{el},2}+\mathcal{E}_{\mathrm{g},2}+\mathcal{E}_\gamma \tag{5.9}$$

subjected to two geometrical constraints $\kappa_1=\beta/D$ and $R=D(\sin\beta/\beta\sin\alpha)$, and to the drop volume conservation $V=V_0$. The first two constraints are used to eliminate κ_1 and R from the variables, leading to an energy that is the function of three variables: $\mathcal{E}=\mathcal{E}(\alpha,\beta,\kappa_2)$.

(*b*) *Results*

We first study equilibrium solutions and their stability for different values of the parameters. Using L_{ec} as unit-length and EI/L_{ec} as unit-energy, the problem has four independent parameters: L, D, $L_{\mathrm{eg}}^3=EI/(\rho gS)$ and $V=wA_{\mathrm{c}}$ the volume of the drop, with A_{c} being given by equation (3.3) with $\kappa=\kappa_1$. We introduce the

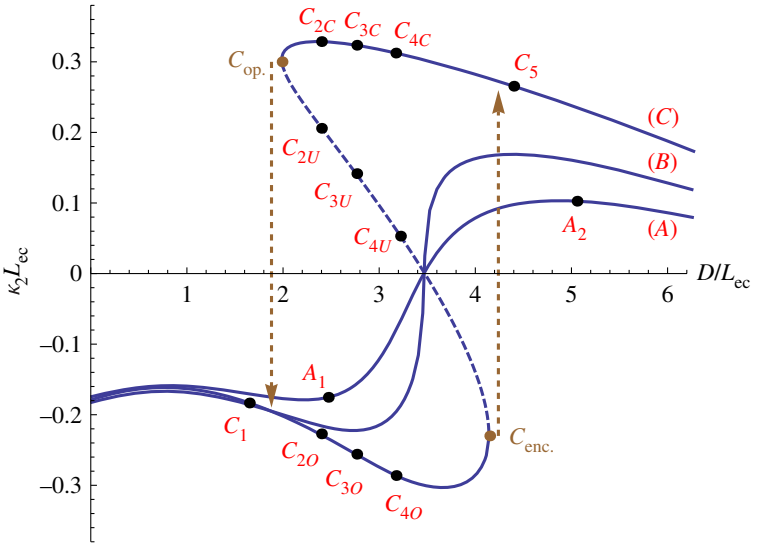

Figure 9. Bifurcation diagram for the drop-strip system of figure 8. Solid (respectively dotted) paths correspond to stable (respectively unstable) states. On each path, the length L is fixed, with $L/L_{ec} = 14$ for path (A), 16 for path (B) and 20 for path (C). Instabilities occurring at fold points $C_{enc.}$ and $C_{op.}$ are indicated by arrows. Fixed parameters are $R_0/L_{ec} = 2$, $L_{eg}/L_{ec} \simeq 6.51$. (Online version in colour.)

equivalent radius R_0 such that $V_0 = \pi w R_0^2$, and use the parameter R_0 instead of V_0. We therefore use the following Lagrangian

$$\mathcal{L}(\alpha, \beta, \kappa_2) = \mathcal{E}(\alpha, \beta, \kappa_2) - \lambda(A_c(\alpha, \beta) - \pi R_0^2) \tag{5.10}$$

and study equilibrium and stability as explained in §2. Results for $R_0/L_{ec} = 2$, $L_{eg}/L_{ec} \simeq 6.51$ are shown in figure 9, where the curvature κ_2 is plotted as a function of the extent of the wet region D. Configurations with negative κ_2 are called *open* (see e.g. configuration A_1 in figure 10), and configurations with positive κ_2 are called *encapsulated* or *closed* (see e.g. configuration A_2 in figure 10). For each value of the three different lengths L/L_{ec}=14, 16 and 20 chosen, we start with an open configuration having small D (e.g. configuration A_1 or C_1 in figure 10). On the one hand, we see in figure 9 that curve (A) contains only stable configurations, which means that in the case of small lengths, increasing D gradually leads to encapsulated configurations without going through instability. On the other hand, we see that curve (C) contains both stable and unstable configurations. Hence, in the case of large lengths, increasing D leads to an instability at the fold point $C_{enc.}$, where the system jumps from being open to encapsulated. If one were to decrease D from that point, the way back would be different with an opening instability happening at the other fold point $C_{op.}$, i.e. hysteresis would be observed. This phenomenon is the signature of a cusp catastrophe (Poston & Stewart 1996). To illustrate this, we plot in figure 11 the loci of the fold points $C_{enc.}$ (upper curve) and of the fold points $C_{op.}$ (lower curve), both curve meeting at the cusp point $(L, D)/L_{ec} \simeq (16.1, 3.46)$, near curve (B). The encapsulating (respectively,

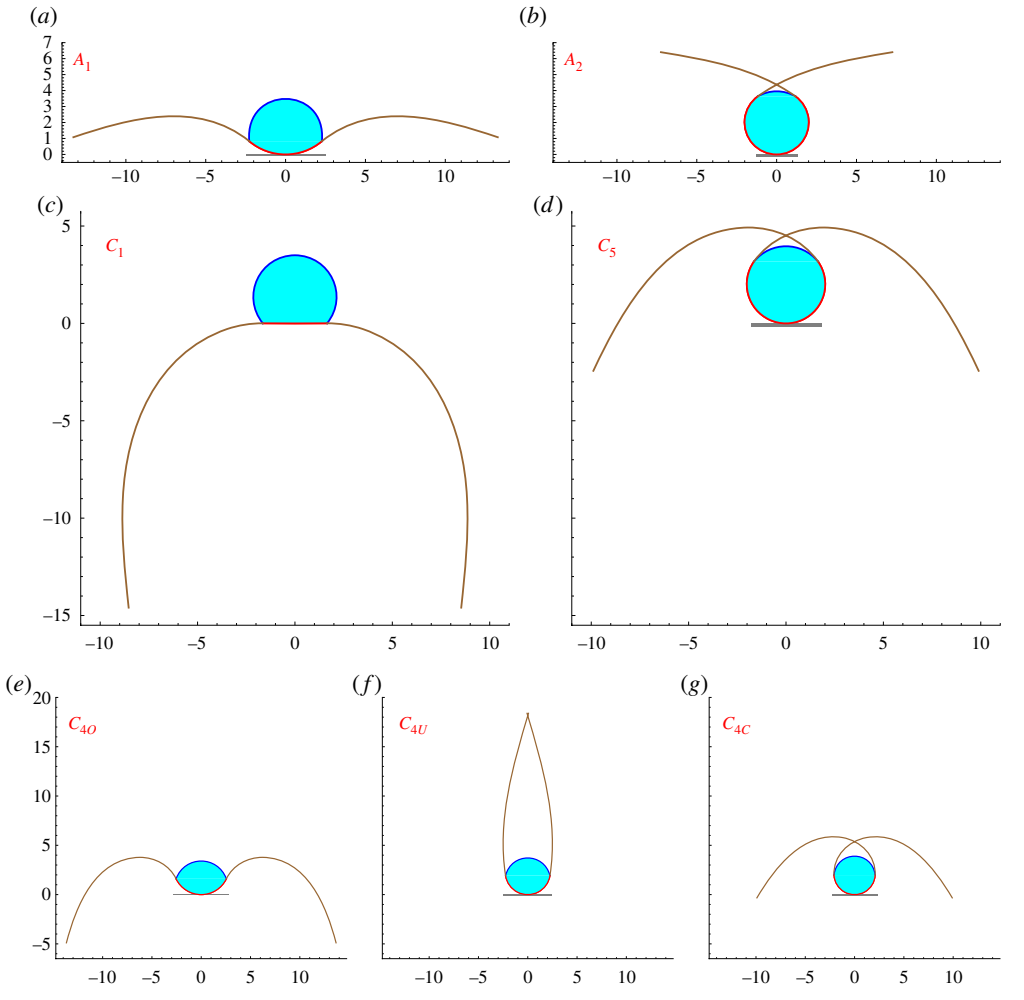

Figure 10. Equilibrium shapes for the drop-strip system of figure 8 for the points (*a*) A_1, (*b*) A_2, (*c*) C_1, (*d*) C_5, (*e*) C_{4O}, (*f*) C_{4U}, and (*g*) C_{4C} of figure 9. Fixed parameters are $R_0/L_{ec} = 2$, $L_{eg}/L_{ec} \simeq 6.51$. The length is $L/L_{ec} = 14$ for configurations A_i, and $L/L_{ec} = 20$ for configurations C_i. All configurations are stable, expect C_{4U}. (Online version in colour.)

opening) instability happens when the system crosses the ($SI_{enc.}$) (respectively ($SI_{op.}$)) curve towards low L values (see arrows in figure 11).

We now investigate how these two curves change when the volume of the drop (i.e. R_0) and the weight of the elastic strip (i.e. L_{eg}) vary. We compute these two curves for various values of R_0/L_{ec} in the range $1.2 \leq R_0/L_{ec} \leq 4$ and of L_{eg}/L_{ec} in the range $200^{1/3} \leq L_{eg}/L_{ec} \leq 10\,000^{1/3}$ and plot them in figure 12. The axes of the figure have been re-scaled in such a way that the (nearly 50) curves approximately collapse on a master curve. We conclude that (i) if $(L - D)/L_{eg} \lesssim 2$, only one equilibrium solution exits and no instability occurs; (ii) if $2 \lesssim (L - D)/L_{eg} \lesssim 3.3$, one or two equilibrium states can exist and instabilities can occur; and (iii) if $3.3 \lesssim (L - D)/L_{eg}$, two states exist and no instability occurs. These instabilities are quasi-static instabilities occurring when a parameter (e.g. D or L) is slowly varied.

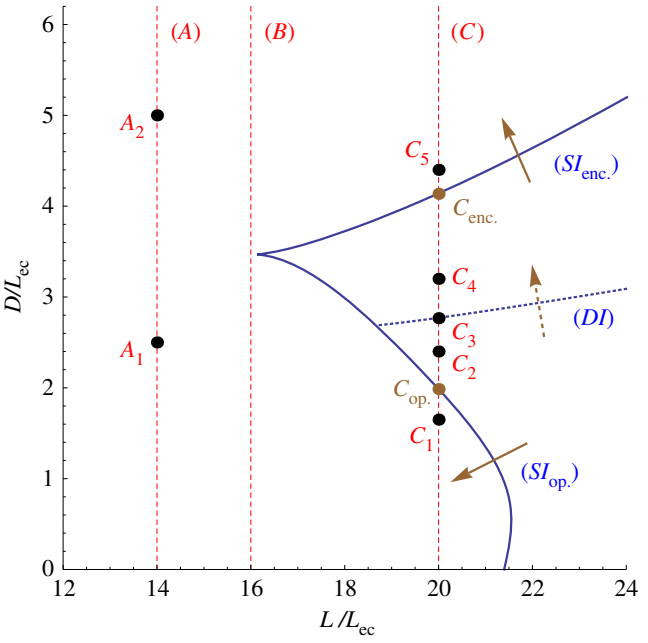

Figure 11. Phases diagram for the drop-strip system of figure 8. The vertical dotted lines correspond to the paths in figure 9. The lower (respectively upper) solid curve $SI_{op.}$ (respectively $SI_{enc.}$) corresponds to fold points where opening (respectively encapsulation) occurs. The dotted curve DI corresponds to the locus of dynamic instability. Fixed parameters are $R_0/L_{ec} = 2$, and $L_{eg}/L_{ec} \simeq 6.51$. (Online version in colour.)

We now consider a different kind of set-up where instability in the dynamics occurs. For the same parameter values $R_0/L_{ec} = 2$, $L_{eg}/L_{ec} \simeq 6.51$ and $L/L_{ec} = 20$, we consider a set-up where a drop is deposited on a flat strip. For different values of the extent D of the wetted region, we look for the long time evolution of the system. As in §4, we are in the case of a suddenly applied load (Simitses & Hodges 2006) where instabilities and shape selection are no longer given by stability properties of equilibriums, but rather by energy-level curves and basins of attraction. To illustrate the phenomenon, we plot energy landscapes of the system for several values of D. Using the constraint $A_c(\alpha, \beta) = \pi R_0^2$, we (numerically) eliminate α from the energy $\mathcal{E}(\alpha, \beta, \kappa_2)$ and end up with an unconstrained energy function of only two variables $\mathcal{E} = \mathcal{E}(\beta, \kappa_2)$. For each point C_1–C_5 of figure 11, we plot in figure 13 curves of constant energy level $\mathcal{E}(\beta, \kappa_2) = G$ for several values of the constant G. For each level set plot, stable and unstable equilibrium points are shown, and the level set corresponding to $\mathcal{E}(0, 0) = G_0$ is distinguished. Upon deposition of the drop on the flat strip, the system starts its dynamics at the origin $(\beta, \kappa_2) = (0, 0)$, and owing to dissipation the dynamics may evolve only towards regions where the energy is lower: the evolution is possible only inside the level set G_0, i.e. for points (β, κ_2) such that $\mathcal{E}(\beta, \kappa_2) \leq G_0$. The system will eventually stabilize on (one of) the stable equilibrium point(s) present inside the level set G_0. In case C_1, there is only one stable equilibrium point corresponding to an open configuration. Going to case C_2, we cross the $(SI_{op.})$ curve in figure 11, that is two equilibria are created in a saddle–node bifurcation. The energy plot of

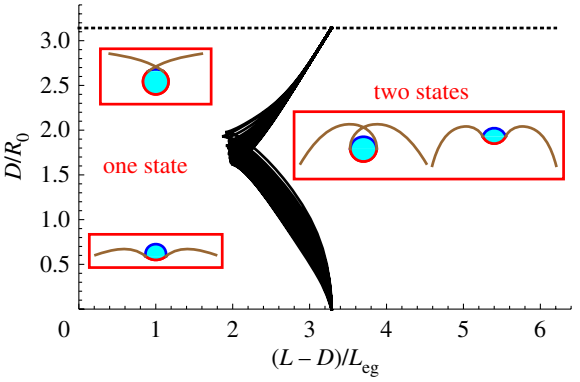

Figure 12. Phases diagram of figure 11 for various values of volume of the liquid drop, $1.2 \leq R_0/L_{ec} \leq 4$ and weight of the strip, $200 \leq (L_{eg}/L_{ec})^3 \leq 10\,000$. The chosen scaling of the axes is such that all the curves nearly collapse of a master curve which separates two regions: on the left only one equilibrium solution exists, whereas on the right two equilibrium solutions coexist. (Online version in colour.)

figure 13*b* therefore exhibits two new equilibria, one stable C_{2C} and one unstable C_{2U}, a saddle point. There are now two competing stable equilibria C_{2C} and C_{2O}, but only C_{2O} lies inside the E_0 level set and therefore the system will stabilizes on this point. As we move from C_2 to C_3 (and further), the level set G_0 encloses wider regions of the (β, κ_2) plane. In case C_3 precisely, G_0 reaches point C_{3U}, giving the system access to the second stable equilibrium point during the dynamics. Consequently, in case C_4, G_0 encloses both C_{4C} and C_{4O} and the dynamics may evolve towards an encapsulated or an open configuration. The value of D corresponding to case C_3 is then the threshold above which the system can evolve towards encapsulation. This new instability from open to encapsulated configurations takes place during the dynamics of the system. We have plotted the locus of this dynamic instability in figure 11, see curve (DI). Going from case C_4 to case C_5, we cross the $(SI_{enc.})$ curve in figure 11, that is the encapsulated and unstable states merge and disappear in a saddle–node bifurcation. Case C_5 in figure 13*e* consequently exhibits only one (stable) equilibrium on which the system always stabilizes.

(*c*) *Discussion*

We have not specifically studied the behaviour of the system during an evaporation experiment, in particular whether an open (respectively, encapsulated) system may become encapsulated (respectively, open) through instability, as evaporation takes place. Partial answer can be sought for in figure 13 where we see that upon evaporation (i.e. decreasing $R_0 = \sqrt{V/(\pi w)}$), an open system initially lying on the right and under the upper instability curve could cross it, thereby experiencing an encapsulation instability. The possibility of encapsulated systems undergoing an opening instability during evaporation remains to be studied.

In the impacting drop experiment of Antkowiak *et al.* (2011), the behaviour of the encapsulation threshold curve as the impact speed U (or Weber number We) vanishes is not given: fig. 3 of Antkowiak *et al.* (2011) stops at $\sqrt{We} \sim 0.4$.

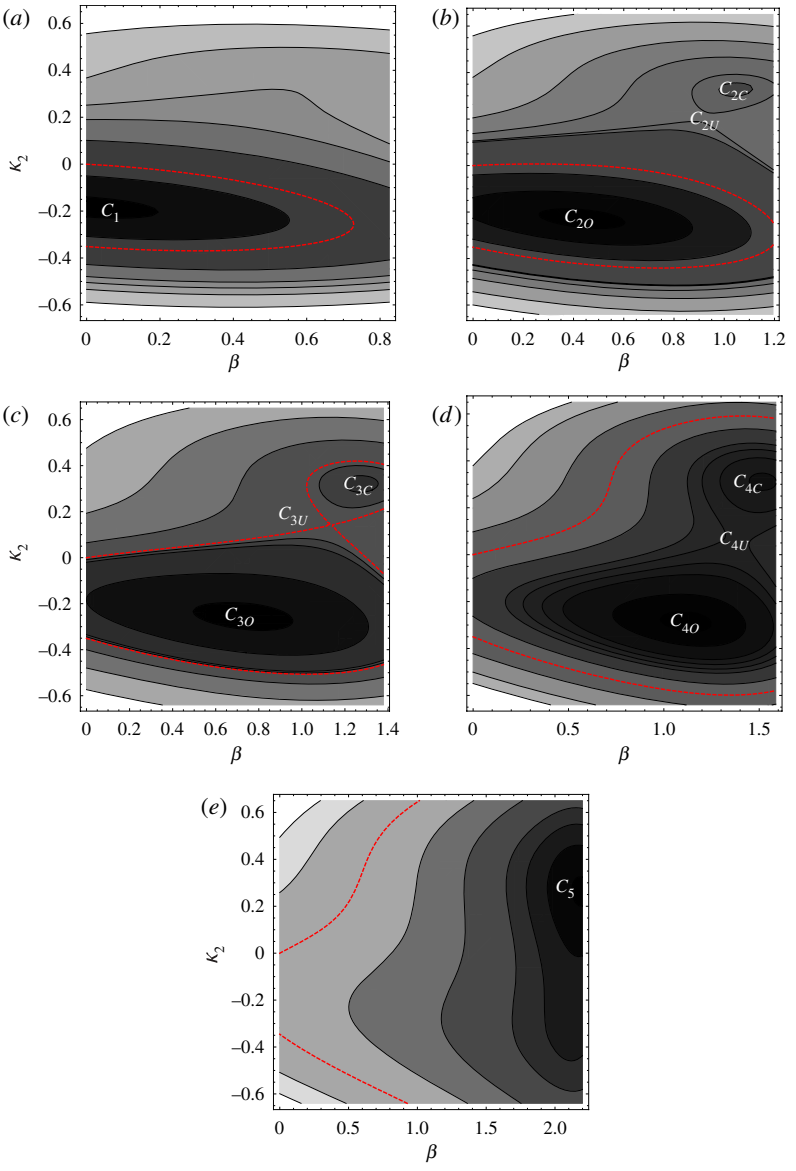

Figure 13. Level sets of the energy $\mathcal{E}(\beta, \kappa_2)$ for the fixed parameters: $R_0/L_{ec} = 2$, $L_{eg}/L_{ec} \simeq 6.51$, and $L/L_{ec} = 20$. The different cases correspond to point (*a*) C_1, (*b*) C_2, (*c*) C_3, (*d*) C_4, and (*e*) C_5 of figure 11. The level set $\mathcal{E}(0,0)$ is drawn in thick dotted lines. (Online version in colour.)

The present results can be used to infer the curve behaviour as $We \to 0$. From equation (4.1), we see that as $We \to 0$ the extent $\Delta = 2D$ of the wetted region goes to Δ_0. On the one hand, if $D = \Delta_0/2$ is larger than the cusp value $D/R_0 \sim 2$, there is a threshold value in L under which the system will encapsulate (given the curve $SI_{enc.}$ or DI of figure 11). Consequently, the behaviour of the encapsulation threshold curve will be as in figure 14*a*. On the other hand, if $D = \Delta_0/2$ is smaller

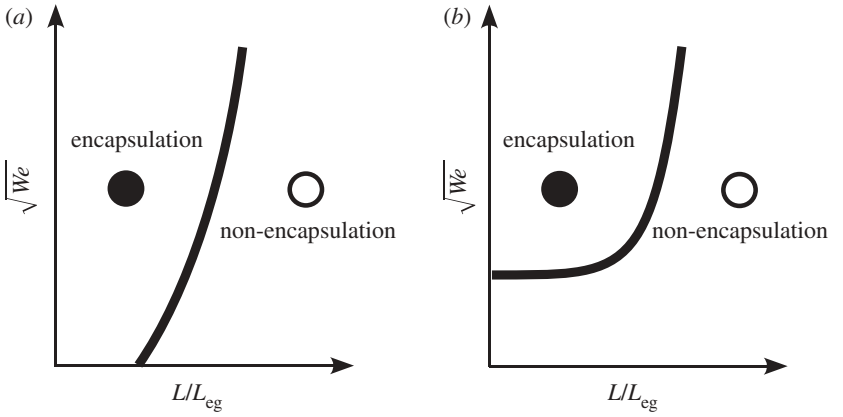

Figure 14. Behaviour of the encapsulation threshold of Antkowiak *et al.* (2011) as the impacting speed vanishes (i.e. small We numbers) (a) in the case where $\Delta_0/2R_0 \gtrsim 2$ and (b) in the case where $\Delta_0/2R_0 \lesssim 2$.

than the cusp value $D/R_0 \sim 2$, no encapsulating instability is possible as the length L is decreased. As a result, the behaviour of the encapsulation threshold curve will be as in figure 14*b*.

Finally, we note that the present discrete model can be extended to include dynamics of the strip by adding the kinetic energy

$$\frac{1}{2}\rho wh \int_{\text{beam}} (\dot{x}^2 + \dot{y}^2)\, \mathrm{d}s \tag{5.11}$$

in the Lagrangian.

6. Conclusion

We have introduced a simplified model for the interaction of an elastic beam with a liquid drop. In the scales considered here, the dominant fluid effect is surface tension, and liquid weight, inertia and viscosity are altogether neglected. The deformations of the elastic beam are also simplified is such a way that equilibrium and stability of the system are found by minimizing a potential energy function of a small number of variables. We have applied our model to three different case studies. In the first one, where a liquid drop bending an elastic strip is let to evaporation, we have found an approximation of the critical length separating the two different behaviours of the system. In the second one, where a drop impacts an elastic strip and depending on the impact speed wrapping of the drop by the strip is achieved or not, we have reproduced the experimental threshold separating encapsulation and non-encapsulation. In the third one, where a drop lifts a heavy elastic strip, we have computed the static and dynamic thresholds for encapsulation, obtaining a universal phases diagram showing the possible states of the system.

We thank A. Antkowiak for discussions. This work was supported by ANR grant no. ANR-09-JCJC-0022-01. Financial support from 'La Ville de Paris - Programme Émergence' is also gratefully acknowledged.

References

Antkowiak, A., Audoly, B., Josserand, C., Neukirch, S. & Rivetti, M. 2011 Instant fabrication and selection of folded structures using drop impact. *Proc. Natl Acad. Sci. USA* **108**, 10 400–10 404. (doi:10.1073/pnas.1101738108)

Aristoff, J. M., Duprat, C. & Stone, H. A. 2011 Elastocapillary imbibition. *Int. J. Nonlinear Mech.* **46**, 648–656. (doi:10.1016/j.ijnonlinmec.2010.09.001)

Bico, J., Roman, B., Moulin, L. & Boudaoud, A. 2004 Adhesion: elastocapillary coalescence in wet hair. *Nature* **432**, 690. (doi:10.1038/432690a)

Brakke, K. A. 1992 The surface evolver. *Exp. Math.* **1**, 141–165.

Clanet, C., Béguin, C., Richard, D. & Quéré, D. 2004 Maximal deformation of an impacting drop. *J. Fluid Mech.* **517**, 199–208. (doi:10.1017/S0022112004000904)

Cohen, A. E. & Mahadevan, L. 2003 Kinks, rings, and rackets in filamentous structures. *Proc. Natl Acad. Sci. USA* **100**, 12 141–12 146. (doi:10.1073/pnas.1534600100)

Duprat, C., Aristoff, J. M. & Stone, H. A. 2011 Dynamics of elastocapillary rise. *J. Fluid Mech.* **679**, 641–654. (doi:10.1017/jfm.2011.173)

Eggers, J., Fontelos, M., Josserand, C. & Zaleski, S. 2010 Drop dynamics after impact on a solid wall: theory and simulations. *Phys. Fluids* **22**, 062101. (doi:10.1063/1.3432498)

de Gennes, P.-G. 1985 Wetting: statics and dynamics. *Rev. Mod. Phys.* **57**, 827–863. (doi:10.1103/RevModPhys.57.827)

Gracias, D. H., Kavthekar, V., Love, J. C., Paul, K. E. & Whitesides, G. M. 2002 Fabrication of micrometer-scale, patterned polyhedra by self-assembly. *Adv. Mater.* **14**, 235–238. (doi:10.1002/1521-4095(20020205)14:3<235::AID-ADMA235>3.0.CO;2-B)

Guo, X., Li, H., Yeop Ahn, B., Duoss, E. B., Hsia, K. J., Lewis, J. A. & Nuzzo, R. G. 2009 Two- and three-dimensional folding of thin film single-crystalline silicon for photovoltaic power applications. *Proc. Natl Acad. Sci. USA* **106**, 20 149–20 154. (doi:10.1073/pnas.0907390106)

Huang, J., Juszkiewicz, M., de Jeu, W. H., Cerda, E., Emrick, T., Menon, N. & Russell, T. P. 2007 Capillary wrinkling of floating thin polymer films. *Science* **317**, 650–653. (doi:10.1126/science.1144616)

Kim, H.-Y. & Mahadevan, L. 2006 Capillary rise between elastic sheets. *J. Fluid Mech.* **548**, 141–150. (doi:10.1017/S0022112005007718)

de Langre, E., Baroud, C. & Reverdy, P. 2010 Energy criteria for elasto-capillary wrapping. *J. Fluids Struct.* **26**, 205–217. (doi:10.1016/j.jfluidstructs.2009.10.004)

Leong, T. G., Lester, P. A., Koh, T. L., Call, E. K. & Gracias, D. H. 2007 Surface tension-driven self-folding polyhedra. *Langmuir* **23**, 8747–8751. (doi:10.1021/la700913m)

Luenberger, D. G. 1973 *Introduction to linear and nonlinear programming*. Reading, MA: Addison-Wesley.

Mastrangeli, M., Abbasi, S., Van Hoof, C., Celis, J.-P. & Bohringer, K. F. 2009 Self-assembly from milli- to nanoscales: methods and applications. *J. Micromech. Microeng.* **19**, 083001. (doi:10.1088/0960-1317/19/8/083001)

Neukirch, S., Roman, B., de Gaudemaris, B. & Bico, J. 2007 Piercing a liquid surface with an elastic rod: buckling under capillary forces. *J. Mech. Phys. Solids* **55**, 1212–1235. (doi:10.1016/j.jmps.2006.11.009)

Poston, T. & Stewart, I. 1996 *Catastrophe theory and its applications*. Mineola, NY: Dover.

Py, C., Reverdy, P., Doppler, L., Bico, J., Roman, B. & Baroud, C. N. 2007 Capillary origami: spontaneous wrapping of a droplet with an elastic sheet. *Phys. Rev. Lett.* **98**, 156103. (doi:10.1103/PhysRevLett.98.156103)

Roman, B. & Bico, J. 2010 Elasto-capillarity: deforming an elastic structure with a liquid droplet. *J. Phys. Condensed Matter* **22**, 493101. (doi:10.1088/0953-8984/22/49/493101)

Simitses, G. J. & Hodges, D. H. 2006 *Fundamentals of structural stability*. New York, NY: Elsevier.

Syms, R. R. A., Yeatman, E. M., Bright, V. M. & Whitesides, G. M. 2003 Surface tension-powered self-assembly of microstructures: the state-of-the-art. *J. Microelectromech. Syst.* **12**, 387–417. (doi:10.1109/JMEMS.2003.811724)

Vella, D., Adda-Bedia, M. & Cerda, E. 2010 Capillary wrinkling of elastic membranes. *Soft Matter* **6**, 5778–5782. (doi:10.1039/c0sm00432d)